Confidence Measures for Assessing the HARP Algorithm in Tagged Magnetic Resonance Imaging

Hanne Kause[1], Aura Hernàndez-Sabaté[4], Patricia Márquez-Valle[4], Andrea Fuster[2,3], Luc Florack[2,3], Hans van Assen[1], and Debora Gil[4]

[1] Department of Electrical Engineering
[2] Department of Biomedical Engineering
[3] Department of Mathematics and Computer Science
Eindhoven University of Technology, The Netherlands

[4] Computer Vision Center, Autonomous University of Barcelona, Spain

h.b.kause@tue.nl

Abstract. Cardiac deformation and changes therein have been linked to pathologies. Both can be extracted in detail from tagged Magnetic Resonance Imaging (tMRI) using harmonic phase (HARP) images. Although point tracking algorithms have shown to have high accuracies on HARP images, these vary with position. Detecting and discarding areas with unreliable results is crucial for use in clinical support systems. This paper assesses the capability of two confidence measures (CMs), based on energy and image structure, for detecting locations with reduced accuracy in motion tracking results. These CMs were tested on a database of simulated tMRI images containing the most common artifacts that may affect tracking accuracy. CM performance is assessed based on its capability for HARP tracking error bounding and compared in terms of significant differences detected using a multi comparison analysis of variance that takes into account the most influential factors on HARP tracking performance. Results showed that the CM based on image structure was better suited to detect unreliable optical flow vectors. In addition, it was shown that CMs can be used to detect optical flow vectors with large errors in order to improve the optical flow obtained with the HARP tracking algorithm.

1 Introduction

Tagged MRI (tMRI) is an important imaging technique to obtain detailed motion information of the cardiac left ventricle (LV) [1]. Tagged MRI images are obtained by spatially modulating the MR magnetization (SPAMM) field just before performing a cine acquisition so that images have a characteristic stripe

or grid pattern that deforms along with cardiac tissue contraction and relaxation [2]. This enables the analysis of motion and deformation over time, which are known to reflect changes due to pathology [3,4,5]. The current standard for obtaining motion information from tMRI is by application of a material point tracking algorithm on harmonic phase (HARP) images, presented by Osman et al. [6,7]. In the past, it has been shown that HARP tracking is able to correctly estimate the displacement of the cardiac muscle [8,9]. Nevertheless, there will always be a limit to the accuracy which may drop in difficult areas. Therefore, it is important to provide an estimate of the upper bound for the error by means of a confidence measure (CM).

In this paper, we test the suitability of two CMs to serve as an estimation of the error bounds in the absence of ground truth. The proposed CMs are quantities computed from the input data that should help detect those points for which the tracking is not accurate enough for further use, such as strain computations. Unreliable points can be selected for post-processing by CMs, which improves the quality of the results. It should be noted that for each value of the confidence measure, which in our case lies within $[0, 1]$, it can only provide an upper bound to the displacement error at each pixel, instead of the displacement error value itself (according to numerical error analysis [10]). This implies that high values of the confidence measure, i.e. high confidence, should ensure a low tracking error, while for low CM values errors may take any value, even a small one. Points that have a high value of the CM and a high error are unpredictable points, which cannot be detected by the CM and, thus, should not occur if the confidence measure has a perfect performance. Furthermore, when this behaviour is stable across frames or references with similar features, the CM is suited for bounding the error in the absence of ground truth, which is ultimately what we need to apply the CMs in a clinical setting.

To the best knowledge of the authors, no confidence measures have been proposed that can give an estimate of the upper bound of the displacement error in HARP results. In this paper, we propose and test the capability of different CMs for bounding the motion estimation error of the HARP algorithm, which is explained in Section 3, while tracking the cardiac left ventricle in tMRI sequences. First, a database of synthetic tagged MR images containing several motion patterns with known ground truth was generated by means of a simplified cardiac motion simulator [11,12] and is analysed with the HARP tracking algorithm. Second, sparse-density plots [13] were used to quantify the capability of a given CM to bound the displacement error within the myocardium. Statistical analysis over the variability of sparse-density plots is used to test the impact of motion and appearance factors in displacement accuracy.

2 Evaluation of Confidence Measures

In this work, the goal of a confidence measure is to provide an upper bound for the flow error in order to detect pixels for which the flow estimation is likely to be non-reliable. In order to assess the capability of a CM for bounding the displacement error, we use Sparse-Density Plots (SDPs) [13]. An SDP evaluates the risk of a confidence measure; that is, the proportion of points (ρ) the bound of which can not be determined by CM values. While decision support systems usually set a lower bound to acceptable accuracy, we compute ρ in terms of the maximum allowed error (E_{max}), which we call risk:

$$\rho(CM_0) := P(E > E_{max}|CM > CM_0). \tag{1}$$

Consequently the SDP is the plot given by:

$$SDP(prct_{CM}) := (prct_{CM}, \rho(prct_{CM})), \tag{2}$$

where $prct_{CM}$ are CM distribution percentiles , which are used instead of directly using the CM to ensure that the SDP is invariant under monotonically increasing transformations of the CM.

Considering a database of image sequences with ground truth, we compute the SDP profile for every two subsequent frames. Note that each SDP profile assesses a bound on the optical flow error specifically for the two frames on which it was based. However, we would like to obtain a general curve, $\mathcal{SDP}$, that can reliably assess a bound on the optical flow error (also called risk) for any other sequence with similar features without ground truth. Therefore, we provide a statistical bound for the risk by computing an upper estimator of SDP profiles using a Student's t-distribution for confident estimation of random variables means. Let us consider a sample of SDP profiles, $\{SDP_i\}_{i=1}^{N}$ of N frames ($N > 30$) presenting similar motion and appearance features. For each CM percentile, $prct_{CM}$, consider the sample mean, $\mu(prct_{CM})$, and variance, $\sigma(prct_{CM})$, computed for the values $\rho_i(prct_{CM})$, $i = 1, \ldots, N$. Then, an upper bound for $\rho_i(prct_{CM})$ at confidence level $\alpha_{\mathcal{SDP}}$ is given by:

$$\mu(prct_{CM}) + t_{1-\alpha_{\mathcal{SDP}}}^{N-1}\sigma(prct_{CM}) = \Upsilon_{prct_{CM}} \tag{3}$$

for $t_{1-\alpha_{\mathcal{SDP}}}^{N-1}$ the value of a Student's t-distribution with N-1 degrees of freedom having a cumulative probability equal to $1 - \alpha_{\mathcal{SDP}}$ [14]. The bounding curve is defined as

$$\mathcal{SDP} := \mathcal{SDP}(prct_{CM}) = (prct_{CM}, \Upsilon_{prct_{CM}})$$

and it indicates that, once a $prct_{CM}$ of pixels has been removed, the error of the remaining ones should be under EE_{max} with probability $\Upsilon_{prct_{CM}}$.

By definition of the confidence interval, the risk at $prct_{CM}$ is under $\Upsilon_{prct_{CM}}$ for new incoming frames with probability $1 - \alpha_{\mathcal{SDP}}$ [14], that is, for approximately $(1 - \alpha_{\mathcal{SDP}})\%$ of frames. For the remaining $\alpha_{\mathcal{SDP}}\%$, the risk could be as high as

1. The bound $\Upsilon_{prct_{CM}}$ applies to all frames provided that SDP variability across such a frame sample is not large [15]. In this context, a most relevant quality feature of confidence measures is a stable behaviour of SDP across sequences in the decision support system. In other words, the lower variability in training SDP profiles we have, the higher predictive value $\mathcal{SDP}$ has.

Under the previous considerations, the capability of a CM for risk bounding should follow a two-stage cascade process. First, $\mathcal{SDP}$ predictive value should be assessed and, then, for those CMs with the highest predictive value, the quality of the bound provided by $\mathcal{SDP}$ should be determined. The predictive value is assessed by the variance of $\mathcal{SDP}$ across the training samples, while the quality of $\mathcal{SDP}$ bound is measured in terms of a minimum risk for the bounded pixels. Each quality score is defined as follows:

1. $\mathcal{SDP}$ **Predictive Value.** Given a sampling of CM-percentiles $prct^j_{CM} = \frac{j \cdot h}{N_{prct}}$, with h the sampling step and N_{prct} the number of percentiles, the variance of its $\mathcal{SDP}$ is approximated by the unbiased sample estimator:

$$\sigma_i^{\mathcal{SDP}} = \frac{1}{N_{prct} - 1} \sum_{j=1}^{N_{prct}} \left(\rho_i(prct^j_{CM}) - \Upsilon^j_{prct_{CM}} \right)^2, \tag{4}$$

   where i and j correspond to the frame and the percentile, respectively, and $\Upsilon^j_{prct_{CM}}$ is the sample mean at the j-th sampled percentile computed by (3).

2. $\mathcal{SDP}$ **Bound Quality.** The amount of risk for a family of SDP curves can be summarized by the mean area, AUC_i^{SDP}, under the curve SDP_i. Given a sampling of CM-percentiles $prct^j_{CM} = \frac{j \cdot h}{N_{prct}}$, AUC_i^{SDP} is defined as:

$$AUC_i^{SDP} := \frac{1}{N_{prct}} \sum_{j=1}^{N_{prct}} \rho_i(prct^j_{CM}) \tag{5}$$

   for i, j denoting the frame and CM-percentile, respectively.

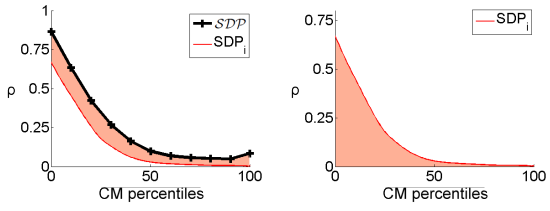

(a) (b)

Fig. 1. CM quality assessment: $\sigma_i^{\mathcal{SDP}}$ computation for $\mathcal{SDP}$ predictive value assessment (a), and AUC_i^{SDP} computation for $\mathcal{SDP}$ bound quality (b).

Figure 1 illustrates the computation of the two quality scores, the variance $\sigma_i^{\mathcal{SDP}}$ and the average risk AUC_i^{SDP}. The prediction curve $\mathcal{SDP}$ is plotted in black and

the SDP_i in red. Subsequently, the variance $\sigma_i^{\mathcal{SDP}}$ is given by the area between both curves (shaded area in Fig.1(a)) whereas the risk AUC_i^{SDP} is given by the area under the curve (shaded area in Fig.1(b)).

3 The HARP algorithm

The stripe or grid pattern that is present in tMRI images deforms along with myocardial tissue contraction and relaxation. This means that via feature tracking, assessment of local cardiac motion should be possible. Osman et al. developed a tracking algorithm (HARP) [6] that links changes of the feature *over time* to local *spatial* feature changes by the tissue displacement $y^{(n+1)} - y^{(n)}$ to be estimated, similar to optical flow [16], but now iteratively:

$$\underbrace{\mathbf{y}^{(n+1)} - \mathbf{y}^{(n)}}_{\text{displacement}} = - \underbrace{[\nabla^* \mathbf{a}(\mathbf{y}^{(n)}, t_{m+1})]}_{\text{(spatial) feature gradient}}^{-1} \underbrace{\mathcal{W}(\mathbf{a}(\mathbf{y}^{(n)}, t_{m+1}) - \mathbf{a}(\mathbf{y}_m, t_m))}_{\text{temporal feature derivative}} . \quad (6)$$

Here, $\mathbf{y}$ is two-dimensional position, n is the iteration number, t_m is time, $\mathbf{a}$ is the *apparent* feature vector $[a_1\ a_2]$, where the subscript determines the input image (image 1 and 2 start with perpendicular stripe tags in the first frame), and $\mathcal{W}$ indicates the apparent feature is wrapped (v.i.).

Typically, the feature tracking in both optical flow and HARP assume feature constancy over time. However, since the intensity of material points is not constant in tMRI images, due to signal decay as a result of T_1-relaxation, intensity is not a proper feature to track. To overcome this issue, Osman et al. developed a tracking algorithm based on (instead of pixel intensity) the harmonic phase of material points, unaffected by signal decay [6].

By application of a Gabor filter to isolate the i-th spectral peak at frequency ω_i in the Fourier domain, a complex-valued spatial domain image is obtained. Usually, the first harmonic spectral peak in the tag direction is preserved. Then, the harmonic phase image is obtained by taking the argument of each pixel in the complex spatial domain image. This is in fact not the true phase ϕ_k but the wrapped "apparent" phase a_k which lies within the interval $[-\pi, \pi)$.

Because $\mathbf{a}$ is wrapped, it has discontinuities, which leads to problems in the context of computing gradients. Therefore, before computing $\nabla \mathbf{a}$, $\mathbf{a}$ is locally unwrapped, indicated by ∇^* in Eq. (6).

4 Experimental Settings

The goal of our experiments is to show the applicability of the framework for selecting CMs capable of predicting the displacement error upper bound in cardiac

tagged MRI sequences analysed with HARP. Since the commercially available HARP software does not allow access to the calculations, we used an in-house implementation of the HARP algorithm described by Osman et. al [6]. In the experiments, we are interested in the displacement of each pixel in the myocardium at each time step and, therefore, we apply the HARP algorithm at each frame separately. In [6], iteration stops when the phase difference between source and target position drops below a threshold. However, since phase error is part of our CM, we did not want to use it as a stopping criterion. Consequently, a stopping criterion based on phase error stability ($\Delta\phi < 0.01$) and/or maximum number of iterations (N=30) was implemented.

The iteration process is stopped when the last five estimates are stable with a threshold of 0.01 or when the maximum number of 30 iterations is reached.

To find the optimal confidence measure for the HARP tracking algorithm, we have considered two types of CMs:

1. Image structure (C_k). The condition numbers of the spatial harmonic phase gradient matrix from each iteration, see Equation (6), defined as

$$C_k = s_{\min}/s_{\max}$$

   where s are singular values [17], are combined by taking the L^2-norm.
2. Energy (C_e). The confidence measure $C_e = \cos(\phi)$ is computed from the final temporal harmonic phase difference

$$\phi = \mathcal{W}(\mathbf{a}(\mathbf{y}_{m+1}, t_{m+1}) - \mathbf{a}(\mathbf{y}_m, t_m)),$$

   which is the difference between the harmonic phases a of the material point in the two frames, with $\mathcal{W}$ a wrapping function, see Equation (6).

4.1 Cardiac Deformation DataSet

In order to test if CMs can accurately bound the motion tracking error, it is necessary to have images with a known motion field. A solution for this is to use artificially generated images. However, to reliably apply the CMs to real data, these synthetic images need to have comparable features to the real clinical images. Therefore, we use the database of synthetic MR images (Fig. 2) first introduced by Márquez-Valle et al. [12], which is based on the cardiac motion simulator by Arts et al. incorporating a time-dependent model using 13 parameters [18].

The datasets contain simulated sinusoidal SPAMM tagged sequences [2], which are modelled with signal decay according to [11]. Different image datasets were created containing either rotation around the long-axis or radially-dependent contraction, while eliminating longitudinal motion in the model to prevent out-of-plane motion in the short-axis images. All seven short-axis slices existed of

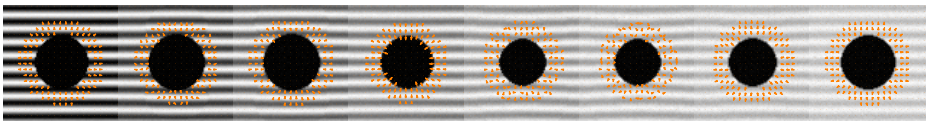

Fig. 2. Every other frame of horizontal tagged sequence from the 3rd slice of the set with contraction. The arrows illustrate a sample of the ground truth and are amplified three times for visibility.

50×50 isotropic pixels and started with the longitudinal axis in the center of the image, see Fig. 2. The cardiac cycle was split into 16 frames and the tagged period was set to 6.6 pixels in either horizontal or vertical direction. Rician noise was added with an SNR of 25, which was constant over time. SNR was defined as $\text{SNR} = \frac{\mu}{\sigma}$ with μ the mean signal and σ the standard deviation of the noise [19]. Signal decay is modelled to mimic the T_1 decay present in MRI. For details on the synthetic data generation, see [12].

4.2 Statistical Analysis

Significance in $\mathcal{SDP}$ variability and bound quality is checked using ANOVA, which is a powerful statistical tool for detecting differences in performance across methodologies as well as the impact of different factors or assumptions. We can apply ANOVA in case our data consists of one or several categorical explanatory variables (called factors) and a quantitative response of the variable. The variability analysis is defined after the ANOVA quantitative score and the different factors and methods are determined. Training data (individuals) is grouped according to such factors, and differences among quantitative response group means are computed. ANOVA provides a statistical way to assess if such differences are significant enough for a given confidence level α. In case of having more than one factor, ANOVA also detects any interaction across the different factors that might distort the analysis of results for each factor separately. If interaction across factors is significant, then the multiple ANOVA has to be re-designed as one factor ANOVA combining all factor groups into a single one to determine whether or not the response variable depends on the combined factors.

The ANOVA design (variable, individuals and factors) for each quality score ($\mathcal{SDP}$ Predictive Value and $\mathcal{SDP}$ Bound Quality) is defined taking as factors the confidence measures (with groups defined by C_e, C_k) and cardiac motions (with groups defined by *Contraction*, *Rotation*). The sampling for each CM quality score is given by $\{\sigma_i^{\mathcal{SDP}}\}_{i=1}^{N_{Fr}}$ and $\{AUC_i^{\mathcal{SDP}}\}_{i=1}^{N_{Fr}}$, respectively. In these experiments the number of frames, N_{Fr}, is set to 40 and they have been randomly sampled across the SA sequences with rotation and contraction motion. To account for non normality in data, ANOVA is performed in logarithmic scale.

5 Results and Discussion

Table 1 shows the average variability (first two columns) and risk (second two columns) for each ANOVA factor group (confidence measures in columns and cardiac motions in rows). For the two quality measures, the 2-way ANOVA over CM and cardiac motions does not detect any significant differences for the motion factor (with $p - Mot = 0.18$ for $\sigma_i^{\mathcal{SDP}}$ and $p - Mot = 0.84$ for $AUC_i^{\mathcal{SDP}}$) nor interaction (with $p - inter = 0.78$ for $\sigma_i^{\mathcal{SDP}}$ and $p - inter = 0.68$ for $AUC_i^{\mathcal{SDP}}$). This implies that the capabilities of each CM for error bounding are independent of the cardiac motion. Conversely, the 2-way ANOVA is significant (with $p - CM = 5 \times 10^{-3}$ for $\sigma_i^{\mathcal{SDP}}$ and $p - CM = 0.005$ for $AUC_i^{\mathcal{SDP}}$) in the column factor and, thus, the capability of C_e and C_k for error bounding is different. In particular, and according to the average values reported in Table 1, we conclude that C_k has a lower variability and risk, regardless of the motion ($p - inter > 0.68$). This is due to the fact that in uniform areas of the image such as the center, interpolation errors are low but HARP cannot compute the phase properly which results in bad correlation.

Table 1. Average variability and risk for each ANOVA factor group.

	$\sigma_i^{\mathcal{SDP}}$		$AUC_i^{\mathcal{SDP}}$	
	C_e	C_k	C_e	C_k
Contraction	2.5×10^{-3}	0.6×10^{-3}	5×10^{-3}	2×10^{-3}
Rotation	7.2×10^{-3}	0.56×10^{-3}	7.3×10^{-3}	2.7×10^{-3}

This is confirmed by a multi comparison test with Tukey correction for one factor given by the two CMs and variable sampling taken for the two motions. The plots of Fig. 3 show the result of the test for $\mathcal{SDP}$ Predictive Value (on the left) and $\mathcal{SDP}$ Bound Quality (on the right). Both plots show intervals for mean differences. Each level mean is represented as a horizontal line centred at the mean group and vertically distributed according to the confidence measure. In the case that there are differences between a selected interval and the others (one in this case), the non-selected intervals are depicted in red.

Note that it is not possible to give a direct and absolute upper bound of the optic flow error. However, since the presented framework uses powerful statistical tools, we are able to provide the risk of unbounded pixels for a specific confidence measure and a sequence with no ground truth. This will enable more reliable interpretation of HARP tracking results. As a next step, pixels with a low confidence could be discarded from the computation and interpolated in the final results. Another option is to include regularisation on the HARP images in the areas with low confidence.

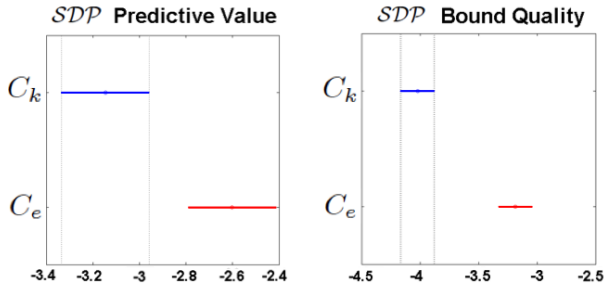

Fig. 3. Multicomparison test for $\mathcal{SDP}$ Predictive Value and $\mathcal{SDP}$ Bound Quality. Results are in logarithmic scale to account for non normality in the data.

Because the synthetic images used in this study accurately simulate the features of real tMRI sequences, we expect that our results translate to real tMRI sequences fairly well. In the future we will apply this framework to clinical images, for which (part of the) optic flow is known[5], in order to prove that these CMs indeed bound the error in clinical images as well.

6 Conclusion

In this paper, we propose and test the capability of two confidence measures for bounding several motion estimation errors of the HARP algorithm in tracking the cardiac left ventricle in tMRI sequences. A 2-way ANOVA over CMs and cardiac motions did not detect any significant differences for the motion factor nor interaction, so that the capabilities of each CM for error bounding are independent of the type of cardiac motion. Furthermore, we concluded that the capability of the CM computed from image structure, C_k, has a better error bounding capability than the CM determined by the energy, C_e. In particular, the phase is not computed properly in noisy areas, which means it cannot correlate well to interpolation error.

References

1. Zerhouni, E.A., Parish, D.M., Rogers, W.J., Yang, A., Shapiro, E.P.: Human heart: Tagging with MR imaging—a method for noninvasive assessment of myocardial motion. Radiology **169**(1) (1988) 59–63
2. Axel, L., Dougherty, L.: MR imaging of motion with spatial modulation of magnetization. Radiology **171**(3) (1989) 841–845
3. Mirsky, I., Pfeffer, J.M., Pfeffer, M.A., Braunwald, E.: The contractile state as the major determinant in the evolution of left ventricular dysfunction in the spontaneously hypertensive rat. Circulation Research **53** (1983) 767–778

[5] A set of volunteer sequences and phantom images are available from the 2011 STACOM challenge. For these images a set of feature points is tracked over time.

4. Götte, M.J., van Rossum, A.C., Twisk, J.W.R., Kuijer, J.P.A., Marcus, J.M., Visser, C.A.: Quantification of regional contractile function after infarction: Strain analysis superior to wall thickening analysis in discriminating infarct from remote myocardium. Journal of the American College of Cardiology **37** (2001) 808–817
5. Delhaas, T., Kotte, J., van der Toorn, A., Snoep, G., Prinzen, F.W., Arts, T.: Increase in left ventricular torsion-to-shortening ratio in children with valvular aorta stenosis. Magnetic Resonance in Medicine **51** (2004) 135–139
6. Osman, N.F., Kerwin, W.S., McVeigh, E.R., Prince, J.L.: Cardiac motion tracking using CINE harmonic phase (HARP) magnetic resonance imaging. Magnetic Resonance in Medicine **42**(6) (1999) 1048–1060
7. Osman, N.F., McVeigh, E.R., Prince, J.L.: Imaging heart motion using harmonic phase MRI. IEEE Transactions on Medical Imaging **19**(3) (2000) 186–202
8. Sampath, S., Derbyshire, J.A., Atalar, E., Osman, N.F., Prince, J.L.: Real-time imaging of two-dimensional cardiac strain using a harmonic phase magnetic resonance imaging (harp-mri) pulse sequence. Magnetic Resonance in Medicine **50** (2003) 154?163
9. Kraitchman, D.L., Sampath, S., Castillo, E., Derbyshire, J.A., Boston, R.C., Bluemke, D.A., Gerber, B.L., Prince, J.L., Osman, N.F.: Quantitative ischemia detection during cardiac magnetic resonance stress testing by use of fastharp. Circulation **107** (2003) 2025–2030
10. Cheney, W., Kincaid, D.: Numerical Mathematics and Computing, Sixth edition. Bob Pirtle, USA (2008)
11. Waks, E., Prince, J.L., Douglas, A.S.: Cardiac motion simulator for tagged MRI. In: Workshop on Mathematical Methods in Biomedical Image Analysis (MMBIA '96). (1996) 0182
12. Márquez-Valle, P., Kause, H., Fuster, A., Hernàndez-Sabaté, A., Florack, L., Gil, D., van Assen, H.: Factors affecting optical flow performance in tagging magnetic resonance imaging. STACOM 2014 (2015) 231–238
13. Márquez-Valle, P., Gil, D., Hernàndez-Sabaté, A.: Evaluation of the capabilities of confidence measures for assessing optical flow quality. International Conference on Computer Vision - Workshops (2013)
14. Fisher, R.: Statistical Methods and Scientific Inference. Oliver and Boyd (1956)
15. Newbold, P., Carlson, W., Thorne, B.: Statistics for Business and Economics. Pearson Education (2007)
16. Van Assen, H., Florack, L., Simonis, F., Westenberg, J., Strijkers, G.: Cardiac strain and rotation analysis using multi-scale optical flow. In Wittek, A., Nielsen, P.M.F., Miller, K., eds.: Computational Biomechanics for Medicine V, Springer-Verlag (2010) 89–100
17. Márquez-Valle, P., Gil, D., Hernàndez-Sabaté, A.: A complete confidence framework for optical flow. Volume 7584 of LNCS., Springer (2012) 124–133
18. Arts, T., Hunter, W., Douglas, A., Muijtjens, A., Reneman, R.: Description of the deformation of the left ventricle by a kinematic model. Journal of Biomechanics **25**(10) (1992) 1119–1127
19. Gutberlet, M., Schwinge, K., Freyhardt, P., et al.: Influence of high magnetic field strengths and parallel acquisition strategies on image quality in cardiac 2D CINE magnetic resonance imaging. Eur Radiol **15**(8) (2005) 1586–97